A Mutation in the 5′-UTR of *IFITM5* Creates an In-Frame Start Codon and Causes Autosomal-Dominant Osteogenesis Imperfecta Type V with Hyperplastic Callus

Oliver Semler,[2,11] Lutz Garbes,[1,4,7,11] Katharina Keupp,[1,4,8,11] Daniel Swan,[3] Katharina Zimmermann,[1] Jutta Becker,[1] Sandra Iden,[8] Brunhilde Wirth,[1,4,7] Peer Eysel,[5] Friederike Koerber,[6] Eckhard Schoenau,[2] Stefan K. Bohlander,[9,10] Bernd Wollnik,[1,4,8] and Christian Netzer[1,*]

Osteogenesis imperfecta (OI) is a clinically and genetically heterogeneous disorder associated with bone fragility and susceptibility to fractures after minimal trauma. OI type V has an autosomal-dominant pattern of inheritance and is not caused by mutations in the type I collagen genes *COL1A1* and *COL1A2*. The most remarkable and pathognomonic feature, observed in ~65% of affected individuals, is a predisposition to develop hyperplastic callus after fractures or surgical interventions. To identify the molecular cause of OI type V, we performed whole-exome sequencing in a female with OI type V and her unaffected parents and searched for de novo mutations. We found a heterozygous de novo mutation in the 5′-untranslated region of *IFITM5* (the gene encoding Interferon induced transmembrane protein 5), 14 bp upstream of the annotated translation initiation codon (c.−14C>T). Subsequently, we identified an identical heterozygous de novo mutation in a second individual with OI type V by Sanger sequencing, thereby confirming that this is the causal mutation for the phenotype. IFITM5 is a protein that is highly enriched in osteoblasts and has a putative function in bone formation and osteoblast maturation. The mutation c.−14C>T introduces an upstream start codon that is in frame with the reference open-reading frame of *IFITM5* and is embedded into a stronger Kozak consensus sequence for translation initiation than the annotated start codon. In vitro, eukaryotic cells were able to recognize this start codon, and they used it instead of the reference translation initiation signal. This suggests that five amino acids (Met-Ala-Leu-Glu-Pro) are added to the N terminus and alter IFITM5 function in individuals with the mutation.

Osteogenesis imperfecta (OI [MIM 166200, 166210, 259420, 166220, 610967, 613982, 610682, 610915, 259440, 613848, 610968, and 613849 for type I to XII of the disease]) is a clinically and genetically heterogeneous disorder associated with bone fragility and susceptibility to fractures after minimal trauma. Some individuals with OI also have hearing loss, dentinogenesis imperfecta, hypermobility of joints, and/or blue sclera. The original Sillence classification, introduced in 1979, uses clinical and radiological features to differentiate between four types: OI type I (mild nondeforming, with blue sclera), type II (perinatal lethal), type III (progressive deforming), and type IV (moderately deforming, with normal sclera).[1] The majority of individuals with the clinical diagnosis OI types I–IV have heterozygous mutations in one of the two genes encoding the α chains of collagen type 1, *COL1A1* (MIM 120150) and *COL1A2* (MIM 120160). OI types I–IV are inherited in an autosomal-dominant manner, and the mutations result in quantitative and/or qualitative defects in type 1 collagen production by osteoblasts.[2–5]

A substantial number of persons with OI do not have a mutation in one of the collagen genes. Many of these are individuals with recessive mutations in a growing list of genes that encode proteins involved in, among other activities, the posttranslational processing or modification of type 1 collagen (*CRTAP* [MIM 605497],[6] *LEPRE1* [MIM 610339],[7] *PPIB* [MIM 123841],[8] and *BMP1* [MIM 112264][9,10]), the final quality control of procollagen formation (*SERPINH1* [MIM 600943][11] and *FKBP10* [MIM 607063)][12]), or osteoblast differentiation (*SP7/OSX* [MIM 606633][13]).[14] The molecular pathomechanism leading to OI in individuals with recessive mutations in *SERPINF1* (MIM 172860) is currently unclear.[15,16]

In 2000, a *COL1A1/2*-mutation-negative group of individuals with autosomal-dominant OI was delineated. These individuals had been classified as having OI type IV, but had some clinical features clearly distinguishing them from other persons with OI.[17] They were then categorized as having OI type V. The most remarkable and pathognomonic feature of OI type V, observed in approximately 65% of affected individuals, is a predisposition to develop a hyperplastic callus after fractures or surgical interventions, predominantly in long bones.[18] Other features are a radiodense band at the growth plate and interosseus membrane calcification of the forearms.[17] These

[1]Institute of Human Genetics, University of Cologne, 50931 Cologne, Germany; [2]Children's Hospital, University of Cologne, 50924 Cologne, Germany; [3]Computational Biology Group, Oxford Gene Technology, Oxford OX5 1PF, UK; [4]Center of Molecular Medicine Cologne, University of Cologne, 50931 Cologne, Germany; [5]Department of Orthopaedic and Trauma surgery, University of Cologne, 50937 Cologne, Germany; [6]Department of Radiology, University of Cologne, 50937 Cologne, Germany; [7]Institute of Genetics, University of Cologne, 50674 Cologne, Germany; [8]Cologne Excellence Cluster on Cellular Stress Responses in Aging-Associated Diseases, University of Cologne, 50674 Cologne, Germany; [9]Department of Internal Medicine III, University of Munich Hospital, Campus Grosshadern, 81377 Munich, Germany; [10]Center for Human Genetics, Philipps University Marburg, 35033 Marburg, Germany
[11]These authors contributed equally to this work
*Correspondence: christian.netzer@uk-koeln.de
http://dx.doi.org/10.1016/j.ajhg.2012.06.011.

characteristics are not consistently found in all individuals with OI type V. On polarized light microscopy in individuals with OI type V, an irregular pattern of bone lamellation is seen. Dentinogenesis imperfecta and blue sclera have not been observed, and there is no evidence for altered collagen migration in gel electrophoresis. The pathogenesis of OI type V is unknown.

In our specialized unit for children with OI at the Children's Hospital of the University of Cologne, we have treated one girl (proband 1) and one boy (proband 2) with the classical clinical diagnosis OI type V. Their diagnoses were based on the fact that both had displayed radiologically confirmed episodes of hyperplastic callus formation after low-trauma fractures (Figure 1). In proband 1, there was also a metaphyseal band visible on the distal femur; such a band is another typical radiological finding in individuals with OI V (Figure 1C). In proband 2, callus formation in the tibia developed without a severe fracture, and a biopsy excluded an osteosarcoma. The histological report confirmed reactive callus tissue without signs of malignancy. Neither of the children had a calcified interosseus membrane of the forearm.

The two children exhibited similar clinical symptoms and disease severity, initially classified as OI type IV. There were no intrauterine fractures reported, and birth length and weight were normal. Dentinogenesis imperfecta was not present, and there were no clinical signs of hearing impairment. The sclerae were grayish, and no ophthalmological problems were detected. Both children had recurrent fractures of long bones and vertebral compression fractures with resulting wedge-shaped vertebrae, indicating generally reduced bone stability. Bone mineral density was below the normal range, and both children developed slight bowing of the extremities and short stature during childhood. They were able to walk short distances. For longer distances, they were dependent on a wheelchair or walking aids.

The clinical findings with regard to the two children are summarized in Table 1. No organ system other than the skeletal system was affected. We did not perform biochemical collagen analyses or molecular tests to exclude mutations in genes known to be involved in the pathogenesis of other OI types. The parents of the affected children were healthy, nonconsanguineous, and of German descent, and they had no overt signs of reduced bone mineral density and no history of previous fractures. DXA measurements have not been performed in the parents. There were no other family members affected by OI. Thus, the family histories were compatible with underlying heterozygous de novo mutations in an as-yet-unknown autosomal gene of the two affected children.

To identify the molecular cause of OI type V, we decided to perform whole-exome sequencing in proband 1 and her unaffected parents and to search for de novo mutations. The study was approved by the ethics committee of the Ludwig-Maximilians University of Munich, and written informed consent was obtained from the probands' parents. We used Agilent SureSelect^{XT} All Exon V4 target enrichment and 100 bp paired-end runs on an Illumina HiSeq 2000 according to the manufacturers' protocols. Across the three samples the mean target coverage was

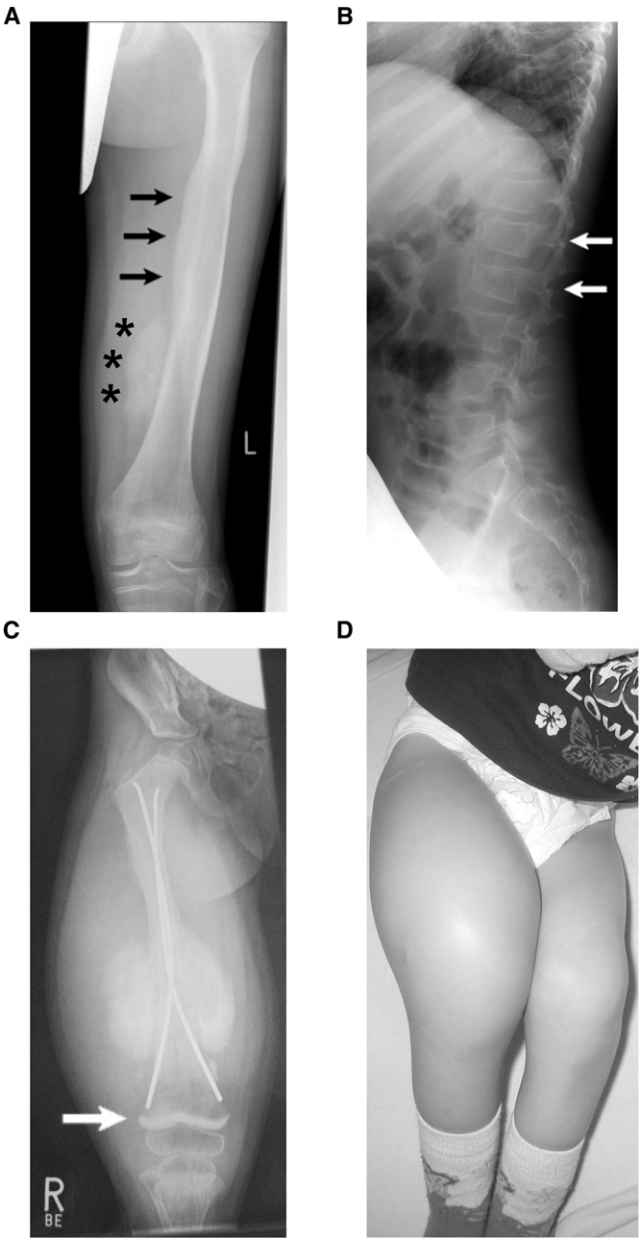

Figure 1. Pictures of the Affected Individuals Enrolled in the Study

(A) Radiograph of the femur of proband 2, showing a thickening of the cortical bone on the medial side (arrows) and a hyperplastic callus at the distal part of the thigh (asterisks).

(B) Radiograph of the lateral spine of proband 2 with signs of vertebral fractures and wedge-shaped and biconcave deformities (arrows).

(C) Radiograph of the right thigh of proband 1 at the age of 2.6 years, showing a hyperplastic callus. At the distal end of the femur, a metaphyseal band (arrow), which is a typical sign of OI type V, is visible. As a result of dislocation of the bone after a fracture, a surgical treatment involving the insertion of two rods was necessary. (D) Photograph documenting the swelling of the right thigh of proband 1.

Table 1. Clinical Features of Two Children with Osteogenesis Imperfecta Type V

Clinical Findings	Proband 1	Proband 2
Disease severity	moderate	moderate
OI type[a]	V	V
Age at first presentation	1 year 7 months	8 years 7 months
Time of follow up	3 years 2 months	6 years 6 months
Hyperplastic-callus formations after fractures before bisphosphonate treatment	yes	yes
Age at start of bisphosphonate treatment	1 year 7 months (iv. neridronate)	9 years 9 months (oral residronate)
Birth length and birth weight	normal	normal
Confirmed prenatal fractures	no	no
Age at first nontraumatic fracture	5 months	18 months
Color of sclera	normal	normal
Dentinogenesis imperfecta	no	no
Hypermobility of joints	no	no
Hearing impairment	no	no
Old fractures of extremities[c]	yes	yes
Spine abnormalities[c]	wedge-shaped vertebrae	biconcave vertebrae
Scoliosis	no	no
Calcified membrane interossea	no	no
Metaphyseal bands	yes	no
Anterior dislocation of the radial head	no	no
Severe bowing of extremities (not due to fractures)	no	no
Age and region of first fracture with hyperplastic callus formation	8 months, right femur	1 year 10 months, forearm
Reduced joint mobility due to callus formations	yes	yes
Weight at first visit kg/BMI (SD) [age]	7.3/15.3 (−0.8) [1.6 years]	25.8/16.5 (0.1) [8.6 years]
Weight at last visit kg/BMI (SD) [age]	12.9/14.0(−1.0) [4.8 years]	45.0/18.9 (−0.4) [15.1 years]
Length at first visit cm (SD) [age]	69 (−2.1) [1.6 years]	123 (−1.8) [1.6 years]
Length at last visit cm (SD) [age]	96 (−2.8) [4.8 years]	154 (−2.4) [15.1 years]
Retarded gross motor functions	delayed standing and walking	no
Mobility at last visit if not limited by fractures (BAMF[b])	7	9
Intelligence	normal	normal
Serum calcium level[c]	normal	normal
Serum alkaline phosphatase[c]	normal	elevated
Serum procollagen type 1 C-peptide[c] (marker for osteoblastic activity)	not measured	normal
Urinary deoxypyridinoline[c] (marker for osteoclastic activity)	elevated	elevated
First available bone density, DXA ap spine (z score) before bisphosphonate treatment	−3.3	−2.8
Last available bone density, DXA ap spine (z score) during bisphosphonate treatment	−1.9	−3.0
Period between DXA measurements	2 years 2 months	6 years 6 months

Abbreviations are as follows: DXA, dual-energy X-ray absorptiometry; ap, anterior-posterior; BMI, body mass index; SD, standard deviation.
[a]According to the expanded Sillence classification.[17]
[b]Brief assessment of motor function.[19]
[c]At first presentation.

59×, and on average, 84% of bases were covered to a minimum depth of 20. Data were analyzed in Oxford Gene Technology's exome analysis pipeline. Briefly, reads were aligned to the reference GRCh37 using *bwa 0.61*.[20] Local realignment was performed around indels with the Genome Analysis Toolkit (GATK v1.4).[21] Optical and PCR duplicates were marked in BAM files with Picard 1.62. Original HiSeq base quality scores were recalibrated with GATK TableRecalibration, and variants were called with GATK UnifiedGenotyper. We hard filtered indels and SNPs according to the Broad Institute's best-practice guidelines (available online) to eliminate false-positive calls. Variant annotation was done with a modified version of ENSEMBL's Variant Effect Predictor.[22]

To determine de novo mutations in the proband, we assessed violations of the Mendelian inheritance rules in the trio by using GATK SelectVariants.[21] A Mendelian violation was scored if the child's genotype differed unexpectedly from that of the known parental genotypes at the same position. This captured positions in which the child (1) harbors an allele that is not present in either parent or (2) is homozygous for an allele present in one but not both parents. To be called as a Mendelian violation, the genotype in the proband and both parents needed to have a minimum genotype QUAL score of 50. QUAL scores are

calculated in the genotyping phase and are the Phred-scaled probability that the polymorphism exists at this site given the underlying sequencing data. The value will increase with greater depth of coverage at the genotype position. All but one of the called Mendelian inconsistancies had read depths of >20 in the proband at the given positions.

Sixteen genes with autosomal variants were thought to contain Mendelian violations. Eleven of the 16 variants were novel, i.e., they were not annotated in dbSNP132, and these were analyzed in more detail. Manual inspection of the genotypes at the read-level revealed that three of the genes with Mendelian violations that were associated with point mutations did not result from the detection of a de novo variant that was detected in the proband but absent in both parents. Rather, they resulted from a putative reversion of this sequence to the reference sequence in the proband for whom one parent was homozygous nonreference. These variants were discarded. Three other Mendelian violations associated with indel positions were rated as artifacts as a result of inconsistencies in the genotype calls in one or both of the parents, a common problem in the course of indel calling in lower-coverage regions. None of the six variants that were discarded affected the coding region of a transcript or a gene with a known function in bone metabolism.

The remaining five variants were followed up by Sanger sequencing of genomic DNA of the proband and her parents. Only one of these variants, a heterozygous C>T transition in the 5′-UTR of *IFITM5* (the gene encoding Interferon induced transmembrane protein 5; NM_00102595.1), affected the transcribed region of a gene, and only two of the candidates were located within genes that have a known function in bone homeostasis: an intronic heterozygous A>C variant in *RUNX1* (MIM 151385, NM_001754.4), located 1307 bp downstream of exon 2, and the *IFITM5* variant. Sanger sequencing revealed that three variants, including the intronic *RUNX1* variant, were false positives. That the *RUNX1* variant was a false positive is well compatible with the whole-exome sequencing data; the *RUNX1* variant call was error prone because of low coverage (10×) in the proband and the variant's genomic location within a repeat region adjacent to a deletion. Two variants were confirmed by Sanger sequencing as true heterozygous de novo mutations in the proband: a variant c.6620-32_-34del in intron 18 of *KIAA0947* (NM_015325.1), encoding a protein of unknown function, and the *IFITM5* 5′-UTR variant, located 14 bp upstream of the annotated translation initiation codon of the gene. The algorithms Splice View[23] and Spliceport[24] did not predict that the intronic variant c.6620-32_-34del in *KIAA0947* would alter the adjacent splice acceptor site.

Therefore, a single de novo mutation in proband 1 remained as a strong candidate for causing the phenotype: the heterozygous variant c.−14C>T in *IFITM5* (Figure 2A and Figure S1). This variant is located in the transcribed region of a gene that encodes a protein with a function in bone. Sanger sequencing of both coding *IFITM5* exons identified no other mutation in the proband. Primer details are available upon request. As a next step, we performed Sanger sequencing of the *IFITM5* 5′-UTR and both coding exons on genomic DNA samples of proband 2 and his unaffected parents. Intriguingly, this individual was heterozygous for the same 5′-UTR mutation c.−14C>T, that we had identified in proband 1, whereas both parents were homozygous for the reference sequence at this site (Figure 2B). Again, no other mutation was detected in the coding region of *IFITM5* in the proband. We confirmed paternity in both proband-parent trios by genotyping 11 microsatellite markers (data not shown; correct paternity in the first proband-parent trio can also be derived from the low number of Mendelian violations in the inheritance of variants). To exclude that this 5′-UTR sequence alteration represents a polymorphism, we referred to the Exome Variant Server (NHLBI Exome Sequencing Project [ESP], Seattle, WA). The genomic position mutated in the two children with OI type V (chr11:299,504 in hg19) was covered in more than 5,150 individuals of European American and African American descent with an average read depth of 14-fold. None of these individuals displayed the *IFITM5* mutation c.−14C>T.

The de novo mutation rate in humans is ~1.1×10^{-8} per position per haploid genome, and there are on average 70 new mutations arising in the diploid genome per generation and 0–3 de novo mutations detectable in the approximately 50 MB of genomic DNA covered by a typical whole-exome sequencing project.[25–27] Therefore, a conservative estimate that takes into account the fact that the *IFITM5* mutation affects a hypermutable cytosine-phosphate-guanine (CpG) dinucleotide would be that the likelihood to detect identical de novo mutations in two individuals with the same phenotype *by chance* is below 5×10^{-6}. We concluded that the *IFITM5* mutation c.−14C>T is the molecular cause of OI type V in both affected children.

IFITM5 (alternatively called Bone-restricted interferon-induced transmembrane protein-like protein [BRIL]) is highly enriched in osteoblasts.[28–30] Its function has mainly been studied in mice and rats. In these animals, *Ifitm5* expression peaks during osteoblast maturation around the early mineralization stage,[28,29] suggesting a role in bone formation. Mouse IFITM5 has a similarity of 88% to human IFITM5.[28] The expression pattern of *Ifitm5* during embryonal development is similar to that observed for *Osterix* (*Sp7*),[29] the human ortholog of which is mutated in a rare autosomal-recessive form of OI.[13] The available expression data from adult rodents argue for a role of *Ifitm5* not only during bone formation in embryogenesis but also during postnatal development. In $Ifitm5^{-/-}$ mice, the long bones are 15%–25% shorter at birth than in $Ifitm5^{+/-}$ mice, and they are sometimes severely bent, a symptom that partially resolves by adulthood.[31] However, bone morphometric parameters for the tibiae did not differ significantly between $Ifitm5^{-/-}$ and $Ifitm5^{+/-}$ mice, suggesting that loss

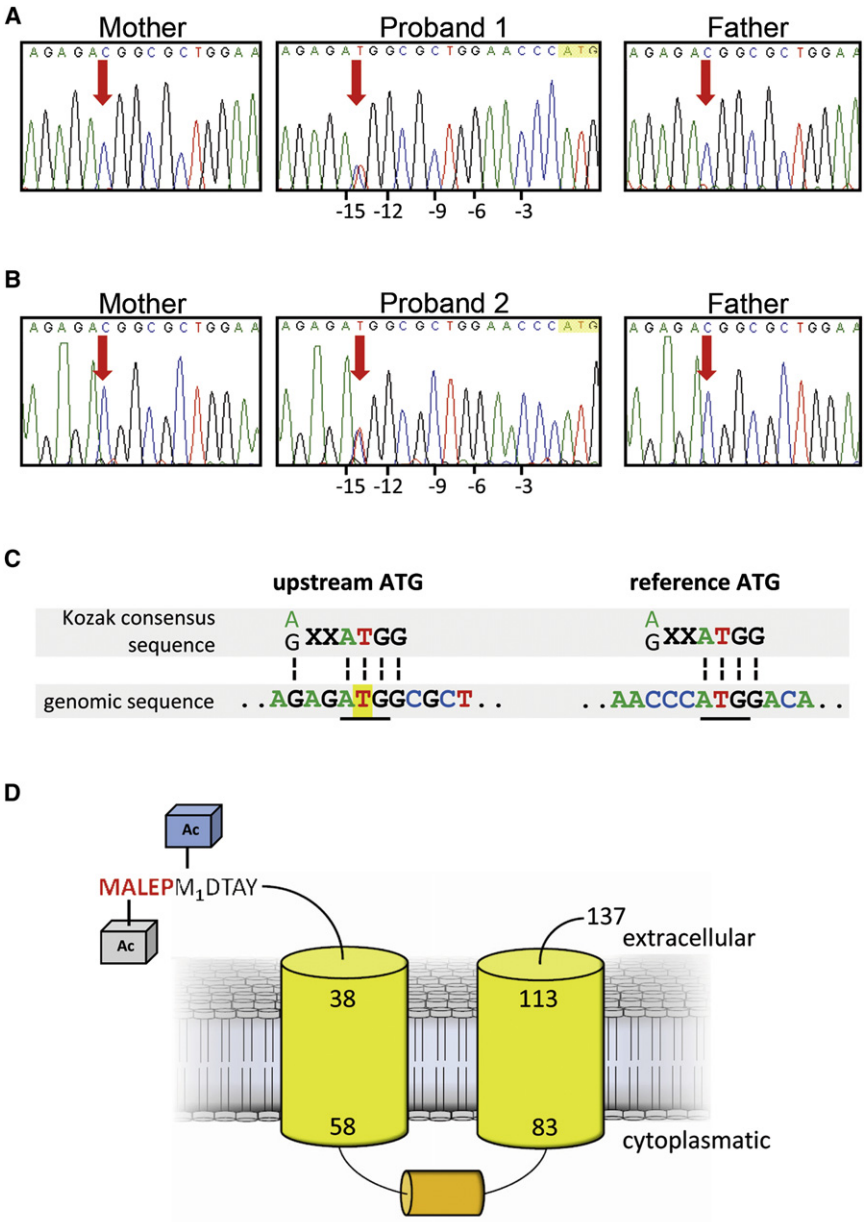

Figure 2. Confirmation of the Heterozygous 5′-UTR *IFITM5* Mutation in the Two Proband-Parent Trios and Prediction of Its Impact on IFITM5

(A) Validation of the *IFITM5* mutation in the 5′-UTR by Sanger sequencing of genomic DNA isolated from peripheral blood. Electropherograms of proband 1 and her parents are shown. The position of the heterozygous c.−14C>T mutation is indicated by the red arrow. The mutation is clearly absent in both parents, confirming its de novo occurrence in proband 1. The bases marked in yellow indicate the position of the reference ATG; numbers indicate the distance to the reference ATG. (B) Identification of the identical *IFITM5* c.−14C>T mutation in proband 2. Electropherograms obtained by Sanger sequencing of genomic DNA of proband 2 and his parents are shown. Again, the mutation is absent in both parents, thereby proving its de novo occurrence. The bases marked in yellow indicate the position of the reference ATG; numbers indicate the distance to the reference ATG. (C) Comparison of the ideal Kozak sequence [A/G]XXATGG with the reference ATG of *IFITM5* and with the newly formed upstream ATG at position −14. In the left part of the diagram, the alignment of the mutated 5′-UTR of *IFITM5* is given, and the alignment of the reference ATG is depicted on the right. Matching bases between the Kozak sequence and the genomic DNA are connected by dashed lines, and the respective ATG codons are underlined. The position of the c.−14C>T mutation is highlighted in yellow. (D) Predicted protein structure of the altered IFITM5. Both transmembrane domains are marked in yellow, and the helical intracellular domain is highlighted in orange. Numbers indicate the amino acids flanking individual domains. The 5 amino acids that would be added by the c.−14C>T mutation are marked in red. The blue and gray boxes indicate the acetyl residue predicted to be added to the wild-type and altered protein, respectively.

of *Ifitm5* has no effect on bone mass. Increased bone fragility or hyperplastic-callus formation has also not been reported for *Ifitm5*-deficient mice. Other bone deficiencies observed in newborn mice, such as a less-calcified mandible and a thinner cranium, disappeared after 5 weeks. The exact function of IFITM5 in the process of bone formation, callus formation, and osteoblast maturation remains to be elucidated. In any case, the available experimental data for the protein argue for a specific function in bones and are therefore well compatible with our genetic finding that mutations in *IFITM5* cause OI type V.

5′-UTR mutations such as the one we identified in *IFITM5* can affect gene expression and protein translation in multiple ways.[32] Among these are aberrant splicing and an altered mRNA secondary structure disrupting proper translation. We found no evidence for such effects of the *IFITM5* c.−14C>T mutation when we used the algorithms Splice View,[23] Spliceport,[24] and RNA fold.[33] An obvious consequence of the heterozygous mutation in the 5′-UTR of *IFITM5* is that it introduces an ATG upstream of the annotated initiation codon for the gene. This upstream ATG is in frame with the *IFITM5* reference open-reading frame (ORF). In general, eukaryotic translation initiation begins at the first AUG embedded into the Kozak consensus sequence [A/G]-XX-AUGG.[34,35] To test whether the AUG formed by the *IFITM5* mutation is embedded into such a Kozak sequence, we used the DNA TIS Miner and the ATGpr algorithms.[36] Both algorithms predicted the AUG created by the mutation to be a stronger start codon than the reference AUG (Figure 2C), implying that

translation initiation in individuals with the mutation would preferentially start upstream of the annotated *IFITM5* ORF. When this upstream AUG is used, five amino acids (Met-Ala-Leu-Glu-Pro) are added to the N terminus of the protein, thereby increasing its size from 137 amino acids to 142 amino acids (Figure 2D).

IFITM5 contains two helical transmembrane domains connected by an intracellular linker (Figure 2D). Both the N and C termini are located at the outer site of the plasma membrane. The MEMSAT[37] script as well as the DOMPRED[38] algorithm predicted that IFITM5 protein structure would not be affected by such an extended N terminus. Next, we concentrated on posttranslational modifications. The algorithms NetNGlyc[39] and NetOGlyc[40] predicted no changes in glycosylation. The TermiNator script[41,42] predicted wild-type IFITM5 to be acetylated at methionine 1 and the altered IFITM5 to be instead acetylated at the novel alanine at position 2 (Figure 2D). Finally, we bioinformatically analyzed whether the localization of the mutated IFITM5 might be altered. Wild-type IFITM5 does not contain a signal peptide guiding it to the plasma membrane, and neither does altered IFITM5, as predicted by the algorithms SignalP[43] and SecretomeP.[44]

Taken together, our bioinformatic analyses strongly suggest that the *IFITM5* mutation leads to the addition of five amino acids to the N terminus of the protein and predicts that the structure and localization of the mutated protein is not impaired. To confirm in vitro that the mutated 5′-UTR sequence is recognized and used as a translation inititation signal in eukaryotic cells, we performed immunoblotting with whole-cell lysates of transiently transfected HEK293T cells overexpressing human *IFITM5* reference mRNA, *IFITM5* mRNA with the mutation c.−14C>T in the 5′-UTR, or *IFITM5* mRNA with this mutation plus a second mutation replacing the reference AUG by the leucine codon CUG (Figure S2). When the expression vector contained the reference 5′-UTR sequence, the C-terminally tagged IFITM5 protein displayed the expected molecular weight of approximately 15 kDa. The mutation c.−14C>T led to the production of IFITM5 with a slightly higher, but clearly distinct, molecular weight (Figure 3). As demonstrated by the transfection of the third construct lacking the reference *IFITM5* start codon, this increased molecular weight resulted from the N-terminal extension of the protein by five amino acids. Thus, the upstream translation initiation signal is used instead of the *IFITM5* reference start codon when both are present in *cis* in eukaryotic cells.

Human disease-causing mutations that occur in the 5′-UTR and create a translation initiation codon are highly uncommon. There are a few published examples of monogenic disorders in which mutations introduce an upstream start codon that is out of frame with the annotated ORF and that thereby reduces the level of the wild-type protein.[45,46] We performed a systematic search of the Human Genome Mutation Database (HGMD)[47] and of the PubMed database and did not identify any 5′-UTR mutation that is known to cause disease through a novel in-frame ATG upstream of the annotated translation start site.

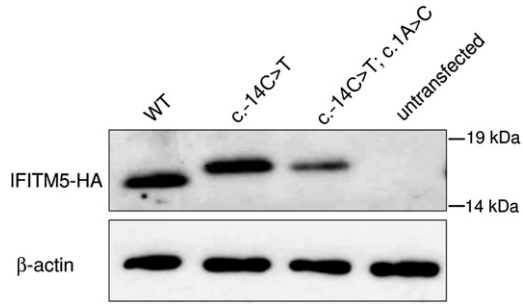

Figure 3. Functional Assay for the c.−14C>T Mutation
HEK293T cells were cultured in Dulbecco's Modified Eagle Media (DMEM, Life Technologies, Darmstadt, Germany) containing 10% fetal bovine serum (FBS, Life Technologies, Darmstadt, Germany) and antibiotics. FuGENE HD transfection reagent (Roche, Mannheim, Germany) was used for transient transfection of these cells either with an *IFITM5* wild-type (WT) expression vector or with one of the construct variants containing the 5′-UTR mutation c.−14C>T. The cells were lysed after 30 hr, and proteins were separated by SDS-PAGE with 4%–12% Bis-Tris gels (Life Technologies, Darmstadt, Germany). Immunoblot analysis with HA antibodies (Roche Diagnostics, Mannheim, Germany) allowed detection of C-terminally tagged IFITM5 (upper panel). Loading of equal protein amounts was confirmed by β-actin detection in the whole-cell lysates (lower panel).

To assess whether the OI type V phenotype results from an IFITM5 gain of function or loss of function, we searched for copy-number variants and chromosomal imbalances encompassing the *IFITM5* locus in the Database of Genomic Variants[48] and the database DECIPHER.[49] The *IFITM5* locus is copy-number stable, but two individuals (probands 250980 and 250982) annotated in DECIPHER had a heterozygous genomic deletion of 320 KB and 440 KB, respectively, which completely deleted *IFITM5* and more than a dozen other genes in this region. The phenotypic description of these individuals includes short stature in proband 250980 and short phalanges, clinodactyly, and microcephaly in proband 250982 as the only skeletal features. The fact that the two individuals obviously did not display bone fragility or hyperplastic-callus formation indicates that haploinsufficiency of *IFITM5* is rather unlikely to play a role in the pathogenesis of OI type V. A dominant-negative effect of the c.−14C>T mutation cannot be formally excluded, but such an effect is not supported by the phenotype observed in *Ifitm5* knock-out mice.[29] From our point of view, the most plausible pathomechanism underlying OI type V is that the addition of five N-terminal amino acids causes a gain of function of IFITM5 by altering the extracellular ligand-binding properties of the receptor. Experimental studies are needed to prove this hypothesis and to dissect the molecular events leading to reduced bone mineral density and hyperplasic-callus formation on the cellular level.

A gain-of-function pathomechanism for OI type V could also explain the remarkable finding of an identical de novo mutation in the two affected individuals. Such a gain of function can be highly specific, thus limiting the mutational spectrum observed for a disorder. A recent example is the somatic activating mutation c.49G>A (p.Glu17Lys) in the oncogene *AKT1* (MIM 164730; NM_001014432.1). This mutation has been identified in a mosaic form in 26 of 29 individuals with Proteus syndrome (MIM 176920), a syndrome characterized by the overgrowth of connective tissue, skin, brain, and other tissues.[50] Sequencing *IFITM5* in larger cohorts of individuals with OI type V will clarify which proportion of cases is caused by the mutation c.−14C>T.

Supplemental Data

Supplemental Data include two figures and are available with this article online at http://www.cell.com/AJHG/.

Acknowledgments

We are grateful to our patients and their parents for participating in this study. We would like to thank Angelika Stabrey for preparing Figure 1, Bärbel Tutlewski for performing the dual-energy X-ray absorptiometry scans, and Monika Kron for administrative support. Whole-exome sequencing was financed by the Jürgen Bierich Award of the Arbeitsgemeinschaft Pädiatrische Endokrinologie to O.S. This work was partially supported by the German Federal Ministry of Education and Research (BMBF) by grant number 01GM0880 (SKELNET) to B.Wo. This study makes use of data generated by the DECIPHER Consortium. A full list of centers that contributed to the generation of the data is available from http://decipher.sanger.ac.uk and via email from decipher@sanger.ac.uk. Funding for the project was provided by the Wellcome Trust. The authors would also like to thank the NHLBI GO Exome Sequencing Project and its ongoing studies, which produced and provided exome variant calls for comparison: the Lung GO Sequencing Project (HL-102923), the WHI Sequencing Project (HL-102924), the Broad GO Sequencing Project (HL-102925), the Seattle GO Sequencing Project (HL-102926), and the Heart GO Sequencing Project (HL-103010). S.I. is supported by Collaborative Research Centers SFB829 and SFB832.

Received: April 21, 2012
Revised: June 5, 2012
Accepted: June 21, 2012
Published online: August 2, 2012

Web Resources

The URLs for data and data analysis presented herein are as follows:

ATGpr, http://atgpr.dbcls.jp/
Broad Institute best-practice guidelines, http://www.broadinstitute.org/gsa/wiki/index.php/Best_Practice_Variant_Detection_with_the_GATK_v3
Database of Genomic Variants (DGV), http://projects.tcag.ca/variation/
DECIPHER (Wellcome Trust Sanger Institute), http://decipher.sanger.ac.uk/
DNA TIS Mine, http://dnafsminer.bic.nus.edu.sg/Tis.html
DOMPRED, http://bioinf.cs.ucl.ac.uk/dompred
Exome Variant Server (NHLBI Exome Sequencing Project, Seattle, WA), http://evs.gs.washington.edu/EVS/
Human Genome Mutation Database (HGMD), http://www.hgmd.org/
IGV browser, http://www.broadinstitute.org/igv
NCBI Reference Sequence (RefSeq), http://www.ncbi.nlm.nih.gov/RefSeq/
MEMSAT, http://bioinf.cs.ucl.ac.uk/psipred/
NetNGlyc, http://www.cbs.dtu.dk/services
NetOGlyc, http://www.cbs.dtu.dk/services
Online Mendelian Inheritance in Man (OMIM), http://www.omim.org
Picard 1.62, http://picard.sourceforge.net/
PubMed, http://www.ncbi.nlm.nih.gov/pubmed/
RNA fold, http://rna.tbi.univie.ac.at/cgi-bin/RNAfold.cgi
SecretomeP, http://www.cbs.dtu.dk/services/SecretomeP
Signal P, http://www.cbs.dtu.dk/services/SignalP/
Spliceport, http://spliceport.cs.umd.edu/
Splice view, http://zeus2.itb.cnr.it/~webgene/wwwspliceview_ex.html
TermiNator, http://www.isv.cnrsgif.fr/terminator3/index.html
UCSC Genome BrowerUniversity, http://www.genome.ucsc.edu

References

1. Sillence, D.O., Senn, A., and Danks, D.M. (1979). Genetic heterogeneity in osteogenesis imperfecta. J. Med. Genet. *16*, 101–116.
2. Barsh, G.S., and Byers, P.H. (1981). Reduced secretion of structurally abnormal type I procollagen in a form of osteogenesis imperfecta. Proc. Natl. Acad. Sci. USA *78*, 5142–5146.
3. Byers, P.H., Tsipouras, P., Bonadio, J.F., Starman, B.J., and Schwartz, R.C. (1988). Perinatal lethal osteogenesis imperfecta (OI type II): A biochemically heterogeneous disorder usually due to new mutations in the genes for type I collagen. Am. J. Hum. Genet. *42*, 237–248.
4. Chu, M.L., Williams, C.J., Pepe, G., Hirsch, J.L., Prockop, D.J., and Ramirez, F. (1983). Internal deletion in a collagen gene in a perinatal lethal form of osteogenesis imperfecta. Nature *304*, 78–80.
5. Williams, C.J., and Prockop, D.J. (1983). Synthesis and processing of a type I procollagen containing shortened pro-alpha 1(I) chains by fibroblasts from a patient with osteogenesis imperfecta. J. Biol. Chem. *258*, 5915–5921.
6. Morello, R., Bertin, T.K., Chen, Y., Hicks, J., Tonachini, L., Monticone, M., Castagnola, P., Rauch, F., Glorieux, F.H., Vranka, J., et al. (2006). CRTAP is required for prolyl 3- hydroxylation and mutations cause recessive osteogenesis imperfecta. Cell *127*, 291–304.
7. Cabral, W.A., Chang, W., Barnes, A.M., Weis, M., Scott, M.A., Leikin, S., Makareeva, E., Kuznetsova, N.V., Rosenbaum, K.N., Tifft, C.J., et al. (2007). Prolyl 3-hydroxylase 1 deficiency causes a recessive metabolic bone disorder resembling lethal/severe osteogenesis imperfecta. Nat. Genet. *39*, 359–365.
8. Barnes, A.M., Carter, E.M., Cabral, W.A., Weis, M., Chang, W., Makareeva, E., Leikin, S., Rotimi, C.N., Eyre, D.R., Raggio, C.L., and Marini, J.C. (2010). Lack of cyclophilin B in osteogenesis

imperfecta with normal collagen folding. N. Engl. J. Med. *362*, 521–528.
9. Asharani, P.V., Keupp, K., Semler, O., Wang, W., Li, Y., Thiele, H., Yigit, G., Pohl, E., Becker, J., Frommolt, P., et al. (2012). Attenuated BMP1 function compromises osteogenesis, leading to bone fragility in humans and zebrafish. Am. J. Hum. Genet. *90*, 661–674.
10. Martínez-Glez, V., Valencia, M., Caparrós-Martín, J.A., Aglan, M., Temtamy, S., Tenorio, J., Pulido, V., Lindert, U., Rohrbach, M., Eyre, D., et al. (2012). Identification of a mutation causing deficient BMP1/mTLD proteolytic activity in autosomal recessive osteogenesis imperfecta. Hum. Mutat. *33*, 343–350.
11. Christiansen, H.E., Schwarze, U., Pyott, S.M., AlSwaid, A., Al Balwi, M., Alrasheed, S., Pepin, M.G., Weis, M.A., Eyre, D.R., and Byers, P.H. (2010). Homozygosity for a missense mutation in SERPINH1, which encodes the collagen chaperone protein HSP47, results in severe recessive osteogenesis imperfecta. Am. J. Hum. Genet. *86*, 389–398.
12. Alanay, Y., Avaygan, H., Camacho, N., Utine, G.E., Boduroglu, K., Aktas, D., Alikasifoglu, M., Tuncbilek, E., Orhan, D., Bakar, F.T., et al. (2010). Mutations in the gene encoding the RER protein FKBP65 cause autosomal-recessive osteogenesis imperfecta. Am. J. Hum. Genet. *86*, 551–559.
13. Lapunzina, P., Aglan, M., Temtamy, S., Caparrós-Martín, J.A., Valencia, M., Letón, R., Martínez-Glez, V., Elhossini, R., Amr, K., Vilaboa, N., and Ruiz-Perez, V.L. (2010). Identification of a frameshift mutation in Osterix in a patient with recessive osteogenesis imperfecta. Am. J. Hum. Genet. *87*, 110–114.
14. van Dijk, F.S., Byers, P.H., Dalgleish, R., Malfait, F., Maugeri, A., Rohrbach, M., Symoens, S., Sistermans, E.A., and Pals, G. (2012). EMQN best practice guidelines for the laboratory diagnosis of osteogenesis imperfecta. Eur. J. Hum. Genet. *20*, 11–19.
15. Becker, J., Semler, O., Gilissen, C., Li, Y., Bolz, H.J., Giunta, C., Bergmann, C., Rohrbach, M., Koerber, F., Zimmermann, K., et al. (2011). Exome sequencing identifies truncating mutations in human SERPINF1 in autosomal-recessive osteogenesis imperfecta. Am. J. Hum. Genet. *88*, 362–371.
16. Homan, E.P., Rauch, F., Grafe, I., Lietman, C., Doll, J.A., Dawson, B., Bertin, T., Napierala, D., Morello, R., Gibbs, R., et al. (2011). Mutations in SERPINF1 cause osteogenesis imperfecta type VI. J. Bone Miner. Res. *26*, 2798–2803.
17. Glorieux, F.H., Rauch, F., Plotkin, H., Ward, L., Travers, R., Roughley, P., Lalic, L., Glorieux, D.F., Fassier, F., and Bishop, N.J. (2000). Type V osteogenesis imperfecta: A new form of brittle bone disease. J. Bone Miner. Res. *15*, 1650–1658.
18. Cheung, M.S., Glorieux, F.H., and Rauch, F. (2007). Natural history of hyperplastic callus formation in osteogenesis imperfecta type V. J. Bone Miner. Res. *22*, 1181–1186.
19. Cintas, H.L., Siegel, K.L., Furst, G.P., and Gerber, L.H. (2003). Brief assessment of motor function: reliability and concurrent validity of the Gross Motor Scale. Am. J. Phys. Med. Rehabil. *82*, 33–41.
20. Li, H., and Durbin, R. (2009). Fast and accurate short read alignment with Burrows-Wheeler transform. Bioinformatics *25*, 1754–1760.
21. DePristo, M.A., Banks, E., Poplin, R., Garimella, K.V., Maguire, J.R., Hartl, C., Philippakis, A.A., del Angel, G., Rivas, M.A., Hanna, M., et al. (2011). A framework for variation discovery and genotyping using next-generation DNA sequencing data. Nat. Genet. *43*, 491–498.
22. McLaren, W., Pritchard, B., Rios, D., Chen, Y., Flicek, P., and Cunningham, F. (2010). Deriving the consequences of genomic variants with the Ensembl API and SNP Effect Predictor. Bioinformatics *26*, 2069–2070.
23. Rogozin, I.B., and Milanesi, L. (1997). Analysis of donor splice sites in different eukaryotic organisms. J. Mol. Evol. *45*, 50–59.
24. Dogan, R.I., Getoor, L., Wilbur, W.J., and Mount, S.M. (2007). SplicePort—An interactive splice-site analysis tool. Nucleic Acids Res. *35*, W285–W291.
25. Keightley, P.D. (2012). Rates and fitness consequences of new mutations in humans. Genetics *190*, 295–304.
26. Roach, J.C., Glusman, G., Smit, A.F., Huff, C.D., Hubley, R., Shannon, P.T., Rowen, L., Pant, K.P., Goodman, N., Bamshad, M., et al. (2010). Analysis of genetic inheritance in a family quartet by whole-genome sequencing. Science *328*, 636–639.
27. Vissers, L.E., de Ligt, J., Gilissen, C., Janssen, I., Steehouwer, M., de Vries, P., van Lier, B., Arts, P., Wieskamp, N., del Rosario, M., et al. (2010). A de novo paradigm for mental retardation. Nat. Genet. *42*, 1109–1112.
28. Moffatt, P., Gaumond, M.H., Salois, P., Sellin, K., Bessette, M.C., Godin, E., de Oliveira, P.T., Atkins, G.J., Nanci, A., and Thomas, G. (2008). Bril: A novel bone-specific modulator of mineralization. J. Bone Miner. Res. *23*, 1497–1508.
29. Hanagata, N., Li, X., Morita, H., Takemura, T., Li, J., and Minowa, T. (2011). Characterization of the osteoblast-specific transmembrane protein IFITM5 and analysis of IFITM5-deficient mice. J. Bone Miner. Metab. *29*, 279–290.
30. Hanagata, N., Takemura, T., Monkawa, A., Ikoma, T., and Tanaka, J. (2007). Phenotype and gene expression pattern of osteoblast-like cells cultured on polystyrene and hydroxyapatite with pre-adsorbed type-I collagen. J. Biomed. Mater. Res. A *83*, 362–371.
31. Hanagata, N., and Li, X. (2011). Osteoblast-enriched membrane protein IFITM5 regulates the association of CD9 with an FKBP11-CD81-FPRP complex and stimulates expression of interferon-induced genes. Biochem. Biophys. Res. Commun. *409*, 378–384.
32. Pickering, B.M., and Willis, A.E. (2005). The implications of structured 5′ untranslated regions on translation and disease. Semin. Cell Dev. Biol. *16*, 39–47.
33. Gruber, A.R., Lorenz, R., Bernhart, S.H., Neuböck, R., and Hofacker, I.L. (2008). The Vienna RNA websuite. Nucleic Acids Res. *36* (Web Server issue), W70–W74.
34. Kozak, M. (1984). Compilation and analysis of sequences upstream from the translational start site in eukaryotic mRNAs. Nucleic Acids Res. *12*, 857–872.
35. Jackson, R.J., Hellen, C.U., and Pestova, T.V. (2010). The mechanism of eukaryotic translation initiation and principles of its regulation. Nat. Rev. Mol. Cell Biol. *11*, 113–127.
36. Nishikawa, T., Ota, T., and Isogai, T. (2000). Prediction whether a human cDNA sequence contains initiation codon by combining statistical information and similarity with protein sequences. Bioinformatics *16*, 960–967.
37. Jones, D.T., Taylor, W.R., and Thornton, J.M. (1994). A model recognition approach to the prediction of all-helical membrane protein structure and topology. Biochemistry *33*, 3038–3049.
38. Marsden, R.L., McGuffin, L.J., and Jones, D.T. (2002). Rapid protein domain assignment from amino acid sequence using predicted secondary structure. Protein Sci. *11*, 2814–2824.

39. Blom, N., Sicheritz-Pontén, T., Gupta, R., Gammeltoft, S., and Brunak, S. (2004). Prediction of post-translational glycosylation and phosphorylation of proteins from the amino acid sequence. Proteomics *4*, 1633–1649.
40. Julenius, K., Mølgaard, A., Gupta, R., and Brunak, S. (2005). Prediction, conservation analysis, and structural characterization of mammalian mucin-type O-glycosylation sites. Glycobiology *15*, 153–164.
41. Martinez, A., Traverso, J.A., Valot, B., Ferro, M., Espagne, C., Ephritikhine, G., Zivy, M., Giglione, C., and Meinnel, T. (2008). Extent of N-terminal modifications in cytosolic proteins from eukaryotes. Proteomics *8*, 2809–2831.
42. Frottin, F., Martinez, A., Peynot, P., Mitra, S., Holz, R.C., Giglione, C., and Meinnel, T. (2006). The proteomics of N-terminal methionine cleavage. Mol. Cell. Proteomics *5*, 2336–2349.
43. Petersen, T.N., Brunak, S., von Heijne, G., and Nielsen, H. (2011). SignalP 4.0: Discriminating signal peptides from transmembrane regions. Nat. Methods *8*, 785–786.
44. Bendtsen, J.D., Jensen, L.J., Blom, N., Von Heijne, G., and Brunak, S. (2004). Feature-based prediction of non-classical and leaderless protein secretion. Protein Eng. Des. Sel. *17*, 349–356.
45. Calvo, S.E., Pagliarini, D.J., and Mootha, V.K. (2009). Upstream open reading frames cause widespread reduction of protein expression and are polymorphic among humans. Proc. Natl. Acad. Sci. USA *106*, 7507–7512.
46. Wethmar, K., Smink, J.J., and Leutz, A. (2010). Upstream open reading frames: Molecular switches in (patho)physiology. Bioessays *32*, 885–893.
47. Stenson, P.D., Ball, E.V., Howells, K., Phillips, A.D., Mort, M., and Cooper, D.N. (2009). The Human Gene Mutation Database: providing a comprehensive central mutation database for molecular diagnostics and personalized genomics. Hum. Genomics *4*, 69–72.
48. Zhang, J., Feuk, L., Duggan, G.E., Khaja, R., and Scherer, S.W. (2006). Development of bioinformatics resources for display and analysis of copy number and other structural variants in the human genome. Cytogenet. Genome Res. *115*, 205–214.
49. Firth, H.V., Richards, S.M., Bevan, A.P., Clayton, S., Corpas, M., Rajan, D., Van Vooren, S., Moreau, Y., Pettett, R.M., and Carter, N.P. (2009). DECIPHER: Database of Chromosomal Imbalance and Phenotype in Humans Using Ensembl Resources. Am. J. Hum. Genet. *84*, 524–533.
50. Lindhurst, M.J., Sapp, J.C., Teer, J.K., Johnston, J.J., Finn, E.M., Peters, K., Turner, J., Cannons, J.L., Bick, D., Blakemore, L., et al. (2011). A mosaic activating mutation in AKT1 associated with the Proteus syndrome. N. Engl. J. Med. *365*, 611–619.